

CrystEngComm

Accepted Manuscript



This is an *Accepted Manuscript*, which has been through the Royal Society of Chemistry peer review process and has been accepted for publication.

Accepted Manuscripts are published online shortly after acceptance, before technical editing, formatting and proof reading. Using this free service, authors can make their results available to the community, in citable form, before we publish the edited article. We will replace this *Accepted Manuscript* with the edited and formatted *Advance Article* as soon as it is available.

You can find more information about *Accepted Manuscripts* in the [Information for Authors](#).

Please note that technical editing may introduce minor changes to the text and/or graphics, which may alter content. The journal's standard [Terms & Conditions](#) and the [Ethical guidelines](#) still apply. In no event shall the Royal Society of Chemistry be held responsible for any errors or omissions in this *Accepted Manuscript* or any consequences arising from the use of any information it contains.

(Submitted to CrystEngComm)

A Simple SVS Way to Obtain Large-scale WO₃ Nanowire Cold Cathode Emitters at Atmospheric Pressure and Low Temperature

Zhuo Xu, Fei Liu*, Daokun Chen, Tongyi Guo, Shunyu Jin, Shaozhi Deng,
Ningsheng Xu, Jun Chen*

State Key Laboratory of Optoelectronic Materials and Technologies, Guangdong Province Key Laboratory of Display Material and Technology, School of Physics and Engineering, Sun Yat-sen University, Guangzhou, China, 510275

**Corresponding email: liufei@mail.sysu.edu.cn; stscjun@mail.sysu.edu.cn*

Abstract

Large scale WO₃ nanowire patterns have been successfully fabricated on a 3.5 inch glass substrate at atmospheric pressure by a simple no-catalyst way. The nanowires were seen to have a mean length of about 40 μm, and their aspect-ratio reaches 200. The nanowires were proven to be single crystalline WO₃ with a monoclinic structure. It is found that the growth region and growth density of the WO₃ nanowires differs with the interval or the width of the W stripes. By combination of designing a series of experiments and analyzing the growth kinetics theory, a novel self-supported vapor-solid (SVS) mechanism is proposed to be responsible for the formation of WO₃ nanowires. Field emission (FE) measurements show that the WO₃ nanowire patterns have excellent FE performances, which have a low turn-on field of 2.9 V/μm and a good field emission uniformity of over 85 %. Moreover, this SVS method may give a helpful reference on low-temperature and no-catalyst growth of other metal oxide nanostructure arrays at atmospheric pressure.

Keywords: Tungsten oxide nanowires, self-supported vapor-solid (SVS) method, atmospheric pressure, no catalyst, field emission

1. Introduction

Metal oxide nanostructures were widely investigated because they have potential applications in optoelectronic area. Among them, tungsten oxide nanowires arouse much attention because they have outstanding photosensitive, gas-sensitive and field emission (FE) performances^[1, 2]. Most reports are concentrated on the controlled growth of WO_x nanowires in past years, using methods such as magnetron sputtering^[3], thermal evaporation^[1, 4-7], sol-gel (solution-gelation)^[8], hydrothermal synthesis^[9] and other chemical solution deposition (CSD) methods ways^[10, 11]. However, there are usually two technical problems for the existing growth methods. One is that most of the preparation methods usually require very high growth-temperature over 700 °C except for the CSD method, which cannot be used in the nanodevices on glass substrate. Another is that large area tungsten oxide nanowire patterns have not been obtained at atmospheric pressure until now. Even for the CSD way, it still fails to fabricate uniform tungsten oxide nanowire patterns. Therefore, to fasten the development of tungsten oxide nanowires in practical applications, these two difficulties must be solved at the same time. It is worthy of being noted that the growth mechanism of tungsten oxide nanowires at a temperature lower than their melting point or sublimation point hasn't been well established, which causes some difficulties in their controlled growth. The existence of these questions provides a great challenge for the researchers.

In this paper, a simple self-supported vapor-solid (SVS) deposition method is used to obtain large-scale WO_3 nanowire patterns on a glass substrate at atmospheric pressure. A new growth mechanism is suggested to explain for the formation of the WO_3 nanowires by combination of experimental results and the growth dynamic theory. In addition, the field emission (FE) properties of patterned WO_3 nanowires are investigated.

2. Experimental

A soda lime glass was used as the substrate. Before the substrate was placed into the reaction furnace, the substrate was respectively cleaned by acetone, ethanol and de-ionized water. Tungsten stripe arrays were prepared on the substrate by combining ultraviolet (UV) lithography with magnetron sputtering techniques. The width of tungsten stripes was 500 μm , and their interval was 120 μm . Schematic diagram of the synthesis steps of the WO_3 nanowire patterns is given in Fig. 1. Firstly, UV photoresist (ZEP-520A, Zeon Corp.) with a thickness of 2 μm was spread to cover the glass substrate. Secondly, a tungsten film with a thickness of 600 nm was deposited on the substrate by magnetron sputtering method. Thirdly, patterned tungsten film was formed by using a lift-off process. Subsequently, the W patterns were put into the furnace and the growth of the WO_3 nanowires began. The temperature was raised to 540 $^\circ\text{C}$ in 1.5 hours and kept here for an hour. The growth pressure was kept at atmospheric pressure. N_2 gas with a flow rate of 2 slm (standard liter per minute) was introduced into the furnace to effectively lower the oxygen content of the system. By lots of experiments, it can be confirmed that the use of Ar or other inert gas also reached the same goal. Moreover, not any catalysts were used in the experiment, which can eliminate the effect of the catalyst sites on the tungsten oxide nanowires and improve their physical property uniformity ^[11]. Finally, the sample was naturally cooled down to room temperature, and a grey-black film was found on the glass substrate.

Scanning electron microscopy (SEM) (Carl Zeiss SUPRA 60) was used to investigate the morphology of the as-prepared WO_3 nanowires. Raman spectrometer (HORIBA LabRAM HR) and transmission electron microscopy (TEM) (FEI Tecnai G2 F30) were applied to analyze their chemical compositions and crystalline structure, respectively.

Results and discussions

By adjusting the experimental parameters, the WO_3 nanowire patterns were fabricated on a 3.5 inch glass substrate. The morphology of the sample is shown in Fig. 2. Large scale nanowire patterns are found to be uniformly distributed on the surface of the glass substrate, and they have a dark blue color from Fig. 2(a). It is seen in Figure 2(b) that the nanowire patterns have a uniform width of $500 \mu\text{m}$ and their interval is about $120 \mu\text{m}$. Nearly all the nanowires are found to only exist in the central regions with a distance of $100 \mu\text{m}$ to the pattern edge rather than the whole surface of the patterns. Top-view and side-view of the nanowires are respectively in Figs 2(d) and 2(e). The length of the tungsten oxide nanowires is observed to range from 10 to $50 \mu\text{m}$, and their averaged diameter is about 120 nm . So the mean aspect ratio of the nanowires is calculated to be around 200. It is also found that the diameter is almost the same throughout the nanowire and its tip is flat, as observed in the inset (Fig. 2(e)). Considering that no catalyst was used in the experiment and the distribution of the nanowire's growth density and morphology are similar for all the patterns, the as-prepared nanowire patterns may have good FE uniformity.

Because tungsten oxides have many phase structures and their XRD peaks were close, X-ray diffraction (XRD) technique is not very suitable to confirm the compositions of the nanowires. Here Raman scattering technique with more sensitivity to tungsten oxide was applied to investigate the chemical compositions of the as-prepared nanowires. Laser with a wavelength of 514.5 nm was used as the excitation source, and typical Raman spectrum of the sample is given in Fig. 3(a). Four characteristic peaks at 135 cm^{-1} , 273 cm^{-1} , 714 cm^{-1} , 808 cm^{-1} are clearly found in the spectrum. Usually, the peak at 135 cm^{-1} results from the lattice deformation^[13], which belongs to the stretching modes. And the peaks at 273 cm^{-1} and 714 cm^{-1} are respectively originated from the O-W-O bending vibration^[14] and W-O-W deformation modes^[15]. And the peak at 808 cm^{-1} should come from the stretching vibrations of the bridging oxygen^[16]. The characteristic Raman peaks of the sample are in a good agreement with those of the WO_3 nanowires in other studies^[13, 14-18], so it can be indexed as the WO_3 phase.

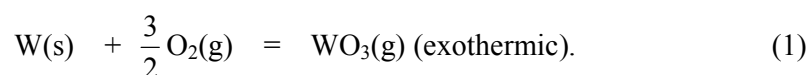
TEM technique was further performed on the sample to analyze the crystalline structure of the nanowires. Typical low- and high-magnification TEM images are respectively indicated in Figs. 3(b) and 3(c). As shown in Fig. 3(b), the diameter of the nanowire is almost the same along its growth direction, which conforms to the observed results in Fig. 2(e). The diffraction spots are clear and sharp in the inset, which suggests the nanowire has good crystallinity. It is also found that some streaking lines can be found in the SAED pattern, which maybe result from the planar defect structures (oxygen vacancies) in the direction normal to the growth direction as depicted in earlier reports^[19, 20]. From Fig. 3(c), one can see that the distance between two adjacent layers is about 0.378 nm along the growth direction. According to the data of the Joint Committee for Powder Diffraction Standards (JCPDS) card No. 20-1324, the nanowire can be confirmed to be is WO₃ single crystal with monoclinic structure grown along the [010] orientation.

In order to achieve the better controllable growth of the WO₃ nanowires using our method, their growth mechanism should be understood. At first, we resorted to the classical vapor-solid (VS) mechanism or vapor-liquid-solid (VLS) mechanism. In the VS process^[21], W or WO_x powders were usually used as the evaporation source. And the growth of WO_x nanowires needed very high temperature over the sublimation-point (1673 K) to generate the vapors^[1, 22, 23]. But in our experiment, the growth temperature was only 540 °C, which was far lower than their sublimation-point. So it is obviously that the VS mechanism can't be applied to interpret the growth of the WO₃ nanowires in our experiment. If the VLS mechanism is adopted^[24], catalyst is essential to the formation of nanowires, which acts as the starting point for the condensing of the hot vapor. The length and the diameter of the nanowires are dependent on the supply of source materials and the size of the catalyst^[6, 25]. However, no catalyst was used in our synthesis process and the length of the nanowires was too long for an hour's growth time, which implies that the possibility of the VLS mechanism is also eliminated.

What leads to the formation of these ultra-long WO₃ nanowires? To solve this question, we designed a series of experiments. Firstly, different W sources were chosen to be the starting materials. When W plate with a thickness of 1 mm was used in our experiment, no nanowires were found on the W surface after an hour's thermal

oxidation at 550 °C, as seen in Fig. 4(a). When a continuous W film with a thickness of 600 nm was used, WO₃ nanoparticle film can be obtained (Fig. 4(b)). But if patterned W stripes with a width of 100 μm were used as the source materials instead of continuous W film or W plate, high-density nanowires with uniform morphology could be clearly found in the centre region of the pattern, as shown in Fig. 4(c). Thus, it was suggested that the use of patterned W film was necessary for the growth of the WO₃ nanowires. Secondly, different widths of W stripes were used as source materials to further explore the growth mechanism. When the width of W films was respectively adjusted to be 500 μm, 250 μm and 70 μm, the morphology of the product varied, as demonstrated in Figs. 5(a)-5(c). It is clearly seen that the growth region of the WO₃ nanowires differed with the width of W stripes. It is noted that whether the width of the W stripe was adopted to be 500 μm or 250 μm, all the nanowires were found to only form at the edge region, which kept a constant distance of about 120 μm to the W stripe center. Moreover, further experiments showed that all the nanowires uniformly distributed on the region with a distance of about 120 μm to the stripe center as long as the stripe width was larger than 240 μm. When the width of the W film was adjusted to be 70 μm, the nanowires are found to distribute at the centre region of the stripe. Although the nanowire distribution region of the sample using 70 μm W stripes was apparently different from that of the samples using a larger width W stripe (>240 μm), the distance between adjacent growth regions of the WO₃ nanowires remained invariable (120 μm). Therefore, it suggests that the length of about 120 μm seems to be a critical distance for the WO₃ nanowires.

Based on these experiment results, we propose a new self-supported vapor-solid (SVS) mechanism, which is schematically illustrated in Fig.6. In our model, the formation of WO₃ nanowires is suggested to be comprised of four thermodynamic stages, which are respectively the evaporation, transportation, nucleation and crystallization. The first growth stage is the evaporation, as described in Fig. 6(a). In initial oxidation reaction, large quantity of reaction heat ^[26] is released and results in the rapid rising of the temperature in some local regions of the W stripes. The thermal oxidation equation can be written as:



Because the formation of WO_3 is exothermic, the releasing heat Q_x can be expressed as

$$Q_x = H \frac{dm}{M} \quad (2)$$

, where x is defined as the distance between some given position and the center of the W stripe (Figure 6(a)), $H(\text{J/mol})$ is the formation enthalpy of the WO_3 , dm is the unit mass of W film, and M is the molar mass of W. According to equation (2), the releasing heat Q_x in the reaction is unvaried with x , which is equal to the heat absorption of unit W film at x position. However, heat loss Q_x' from thermal diffusion effect varies with the position x because different regions in the W stripe have diverse heat transfer ability to the environment. It can be written as:

$$Q_x' = f(x) \propto x. \quad (3)$$

Based on this relationship, the heat loss ($Q_x' \big|_{\text{edge}}$) at stripe edge should be higher than the heat loss ($Q_x' \big|_{\text{centre}}$) at stripe center because the heat transfer of the film edge to the chamber atmosphere is much rapider than that of the film center in an equal time. Both heat absorption and heat loss simultaneously exist in our experiment, so the absolute heat accumulation $Q(x)$ of the W stripe at position x can be expressed as:

$$Q(x) = Q_x - Q_x' = H \frac{dm}{M} - f(x). \quad (4)$$

Heat capacity C of W film can be deduced by classical heat capacity formula^[27]:

$$dT_x = \frac{Q(x)}{C \cdot dm} \quad (5)$$

, where dT_x represents the temperature rise of the W film at x position. Substituting equation (4) into equation (5), we can obtain:

$$dT_x = \frac{H}{C \cdot M} - \frac{f(x)}{C \cdot dm} = A - F(x) \quad (6)$$

, where A stands for the constant $H/(CM)$, and $F(x)$ is the function $f(x)/(Cdm)$. After a thermal oxidation period t is over, the temperature T_x at x position can be approximately deduced by the following equation:

$$T_x = \int_0^t [A - F(x)] dt. \quad (7)$$

When x is adopted to be 0, the temperature T_x at x position becomes the temperature T_c at the W stripe centre, which can be worked out to be At based on equation (7). If we

regard $F(x)t$ as $G(x)$, equation (7) can be expressed as:

$$T_x = T_c - G(x). \quad (8)$$

According to equation (8), the relationship of temperature versus the diffuse distance (T_x - x) can be qualitatively given, as indicated in Fig. 6(a). From the T_x - x curve, it is clearly seen that the temperature (T_c) of the stripe center is the highest and that (T_{edge}) of the stripe edge is the lowest. Because T_c is proportional to the thermal oxidation period t , T_c can reach high temperature over the sublimation point ^[28] of W if the period t is long enough. In this case, the W film will be sublimated to W vapor and subsequently oxidized into WO_3 vapor at the following reaction with O_2 gas.

In the second stage (Figure 6(b)), the transportation of the WO_3 molecules takes place by the driving of the temperature gradient, which comes from the temperature difference between the stripe centre and the stripe edge. In general, the WO_3 transportation should conform to the classical Ficker's second Law:

$$dN = - D \left(\frac{dn}{dx} \right)_x \quad (9)$$

, where dN is the flux density of WO_3 , D is the diffusion constant of WO_3 , and n_x is defined as the number density of the WO_3 molecules at x position, which increases with the evaporation temperature T_x . In our experiment, the gradient of the number density $\left(\frac{dn}{dx} \right)_x$ decreases with the position x because the center temperature of the stripe is higher than the edge region. Therefore, dN is positive, which lead that the WO_3 molecules transport from the centre of W stripes to their edge.

Figure 6(c) gives the third growth step of the WO_3 nanowires. Theoretically, the transportation of WO_3 molecules will not stop until $\left(\frac{dn}{dx} \right)_x$ returns to zero. Based on equation (8), the temperature T_x will decrease with the increase of the transportation distance x of the WO_3 molecules. Considering that the saturation vapor pressure P_0 increases with the temperature T , P_0 will decrease with the transportation distance x . When the vapor pressure P_x at x position is larger than the saturation pressure P_0 , WO_3 molecules will nucleate. Therefore, the transportation distance of the WO_3

molecules should be finite in our experiment. Compared with the experiment results in Fig. 5, it can be concluded that the critical transportation distance of the WO_3 molecules should be about $120\ \mu\text{m}$ in our experiment. It is worth noting that there should have two discrepant development tendencies in the nucleation stage for W stripes with different widths in this stage, which can be respectively found in the left and right image of Fig. 6(c). If the distance d between adjacent stripe centers is larger than $240\ \mu\text{m}$, the WO_3 molecules will nucleate at the edge region with a $120\ \mu\text{m}$ distance to the stripe center because the vapor pressure P_x reaches the saturation pressure P_0 . But if d is smaller than $120\ \mu\text{m}$, the WO_3 molecules will nucleate at the centre of W stripes because the vapor pressure P_x arrives at P_0 under this growth condition. Thus, the aforementioned experiment results (Figure 5(c)) that the growth regions of the nanowires varied with the stripe widths can be well comprehensible by our new model.

The last stage is the crystallization of WO_3 nanowires, as seen in Fig. 6(d). With the proceeding of the reaction, the WO_3 nucleus will grow along the energy favorable direction and form single crystalline WO_3 nanowires. To ensure the sufficient supply of W source and maintain enough growth time of the nanowires, the minimum thickness of W film is $600\ \text{nm}$ and the annealing period should be over an hour based on our experiences. When the reaction is over, the length of the nanowires can reach as long as $50\ \mu\text{m}$ because the transportation distance of WO_3 molecules was very long (about $120\ \mu\text{m}$) based on our SVS mechanism.

By analysis of four growth procedures of the WO_3 nanowires, the WO_3 molecules are completely self-supported without any help from the catalysts or the source materials. In addition, W film acts as both the evaporation source and the substrate in the whole reaction, and thus this growth mechanism is named as the self-supported vapor-solid (SVS) mechanism. Based on this novel SVS mechanism, the growth parameters of the WO_3 nanowires can be optimized. At present, the most suitable width and interval of W stripes are respectively $125\ \mu\text{m}$ and $60\ \mu\text{m}$. As found in Fig. 7(a), the nanowires are very uniform and have the highest aspect ratio (about 200) if these growth parameters are adopted.

To investigate their application future in FE area, field emission (FE) measurements of the sample were carried out in the field emission measurement system, as shown in Fig. 7(a). Here, a diode structure equipped with the sample and the phosphor screen was used to obtain the emission properties of the whole nanowire film simultaneously record their emission images. As seen in Fig. 7(a), a phosphor screen was used as the anode and the nanowire arrays were used as the cathode in experiments. This diode structure has a spacing of 500 μm and the base pressure of the measurement chamber was 5×10^{-5} Pa. Also, the size of the substrate was 3.5 inch, and the total area of W stripe patterns was calculated to be about 8 cm^2 . Typical emission image is shown in Fig. 7(b), in which one can find that both the brightness uniformity and the distribution uniformity of the emission patterns are better than 85 %. The uniform physical property of the nanowires should be responsible for their good FE performance because not any catalysts were used in the experiment. Figure 7(c) is the FE current density versus electric field (J-E) curve of the sample, and the corresponding Fowler-Nordheim (F-N) plots are provided in the inset. As found in Table I, the as-prepared nanowires have a mean turn-on field of 2.9 $\text{V}/\mu\text{m}$ ($J=10 \mu\text{A}/\text{cm}^2$), which is much lower than that most of the tungsten oxide nanowires in previous reports [29-34]. And the maximum current of the nanowire patterns can arrive at 2.5 mA. Emission stability measurement lasts 4000 min at a high emission current of 500 μA to further value the emission performance of the WO_3 nanowires. An emission current fluctuation lower than 8 % can be found in Fig. 7(d), which is good enough for the FED applications. Moreover, the emission behaviors of the as-grown WO_3 nanowires can be comparable to many excellent cathode nanostructures, such as ZnO nanowires, Cu_2O nanocrystals, MoS_2 nanosheets, SiC nanowires, NdB_6 nanowires, CrSi_2 nanowires, TiO_2 nanotubes and Ag nanowires [35-41], which suggests that the WO_3 nanowires by SVS method have great potential FE applications. The possible reasons of their nice FE performances can be depicted as follows. The FE properties of nanomaterials are mainly dependent on the nanowires' growth density, conductivity and aspect ratio. Although there exist a few planer defects in the lattice

of the WO_3 nanowires, they are single crystals with good crystallinity, as seen in Fig. 3(c). Better crystallinity can ensure that they can have relatively higher conductivity, which will lower their turn-on and threshold field. On the other hand, the as-prepared WO_3 nanowires have higher aspect ratio (about 200) and more suitable growth density, which can efficiently increase the field enhancement factor and decrease the field emission screening effect^[5]. The nonlinear behaviors of FN plots have several possible explanations, such as the removing of the adsorbates, burning out the longest ones^[42] or the variety of the field enhancement factor β at applied field^[43,44]. In our experiments, we attribute the nonlinear behavior of the FN plots to the variety of β at applied field due to the following reasons.” We have carefully treated the WO_3 nanowires by a long-term (over 6 hours) and constant-field ($4.4 \text{ V}/\mu\text{m}$) conditioning procedure. Typical J-E curve and FN plots of the sample are given after the conditioning treating was over. Through this treating procedure, the WO_3 nanowires are found to have repeatable and stable emission behaviors, which can be found in Fig. S1 in Supporting Information. In this case, the adsorbates should be thoroughly removed, so this possibility can be eliminated. Moreover, some long nanowires can be burn down in this process, which have a little effect on their emission behaviors. But the β value is dependent on both the length and the radii of the nanowire based on our previous researches^[43,44]. Because the length and the diameter of nanowires by CVD way can't be the same, their β value should be variable to some extent. Only the nanowires with high β value can emit the electrons at lower field. But at high field, all the nanowires with high or low β value involved in the emission. As a result, the emission contribution from the nanowires with different β values leads to the emergence of the nonlinearity of the FN plots.” At present, more efforts are devoted to designing a more suitable mask to enhance their emission behaviors (decreasing the turn-on field and increasing the emission uniformity and stability) of the gated FE devices, which is still in research.

Conclusion

By using W stripes as source materials, large scale WO₃ nanowires have been successfully prepared on the glass substrate at atmospheric pressure. The nanowires are proven to be single crystals with monoclinic structure. Moreover, it is found that the width and interval of W stripes determine the nucleus regions and growth density of the nanowires. A novel SVS growth mechanism is proposed to comprehend the formation of nanowires by combination of the thermodynamic theory and the experimental results. FE results show that patterned WO₃ nanowires have an averaged turn-on field of 2.9 V/ μm and their emission uniformity is over 85 %, which suggests that they should be ideal cathode nanomaterial candidates. This simple synthesis method may shed light on the no-catalyst and atmospheric-pressure growth of other metal oxide nanostructure arrays at low temperature.

Acknowledgements

This work was supported by National Key Basic Research Program of China (Grant No. 2010CB327703, 2013CB933601), the National Natural Science Foundation of China (Grant No. 51072237, 60925001, U1134006), National Project for the Development of Key Scientific Apparatus (2013YQ12034506) of China, the Fundamental Research Funds for the Central Universities (2009-30000-3161452), the Natural Science Foundation of Guangdong Province (No. S2012010010519), and Program for New Century Excellent Talents in University (NCET-12-0573).

References

- [1] J. Zhou, L. Gong, S. Z. Deng, J. Chen, J.C. She, N. S. Xu, R. Yang and Z. L. Wang, *Appl. Phys. Lett.*, 2005, **87**, 223108.
- [2] J. Chen, Y. Y. Dai, J. Luo, Z. L. Li, S. Z. Deng, J. C. She and N. S. Xu, *Appl. Phys. Lett.*, 2007, **90**, 253105.
- [3] C. G. Granqvist, *Sol. Energ. Mater. Sol. C.*, 2000, **60**, 201-262.
- [4] J. Thangala, S. Vaddiraju, R. Bogale, R. Thurman, T. Powers, B. Deb and M. Sunkara, *Small*, 2007, **3**, 890.
- [5] M. Furubayashi, K. Nagato, H. Moritani, T. Hamaguchi and M. Nakao et al., *Microelectron. Eng.*, 2010, **87**, 1594.
- [6] F. Liu, L. Li, F. Y. Mo, J. Chen, S. Z. Deng and N. S. Xu, *Cryst. Growth Des.*, 2010, **10**, 5193.
- [7] F. Liu, T. Y. Guo, Z. Xu, H. B. Gan, L. F. Li, J. Chen, S. Z. Deng, N. S. Xu, D. Golberg and Y. Bando, *J. Mater. Chem.C*, 2013, **1**, 3217.
- [8] C. Santato, M. Odziemkowski, M. Ulmann and J. Augustynski, *J. Am. Chem. Soc.*, 2001, **123**, 10639.
- [9] H. Kominami, K. Yabutani, T. Yamamoto, Y. Kara and B. Ohtani, *J. Mater. Chem.*, 2001, **11**, 3222.
- [10] W. H. Lai, J. Shieh, L. G. Teoh and M. H. Hon, *Nanotechnology*, 2006, **17**, 110.
- [11] X. L. Li, T. J. Lou, X. M. Sun and Y. D. Li, *Inorg. Chem.*, 2004, **43**, 5442.
- [12] F. Liu, Z. J. Su, L. Li, F. Y. Mo, S. Y. Jin, S. Z. Deng, J. Chen, C. M. Shen, H. J. Gao and N. S. Xu, *Adv. Funct. Mater.* 2010, **20**, 1994.
- [13] J. Díaz-Reyes, V. Dorantes-García, A. Pérez-Benítez and J. A. Balderas-López, *Superficies y Vacío*, 2008, **21**, 12.
- [14] A. Raouigier, F. Portemer, A. Quede and M. El Marssi, *Appl. Surf. Sci.*, 1999, **153**, 1.
- [15] J. Pfeifer, C. Guifang, P. Tekula-Buxbaum, B. A. Kiss, M. Farkas-Jahnke and K. Vadasdi, *J. Solid State Chem.*, 1995, **119**, 90.
- [16] P. Tagtstrom and U. Jansson, *Thin Solid Films*, 1999, **352**, 107.
- [17] D. Y. Lu, J. Chen, J. Zhou, S. Z. Deng, N. S. Xu and J. B. Xu, *J. Raman Spectrosc.*, 2007, **38**, 176-180.
- [18] H. D. Zheng, J. Z. Ou, M. S. Strano, R. B. Kaner, A. Mitchell, and K. Kalantar-zadeh, *Adv. Funct. Mater.*, 2011, **21**, 2175.
- [19] J. Zhou, Y. Ding, S. Z. Deng, L. Gong, N. S. Xu and Wang, Z. L., *Adv. Mater.* 2005, **17**, 2107.
- [20] J. Thangala, Z. Q. Chen, A. Chin, C. Z. Ning and M. K. Sunkara, *Cryst. Growth Des.*, 2009, **9**, 3177.

- [21] W. Z. Pan, Z. R. Dai and Z. L. Wang, *Science*, 2001, **291**, 1947.
- [22] L. Li, Y. Zhang, X. S. Fang, T. Y. Zhai, M. Y. Liao, X. L. Sun, Y. Koide, Y. Bando and D. Golberg, *J. Mater. Chem.*, 2011, **21**, 6525.
- [23] Lamartine Meda, Aaron M. Dangerfield, Mila'na C. Jones, Christian M. White and Anantharamulu Navulla, *Jpn. J. Appl. Phys.*, 2012, **51**, 6.
- [24] A. M. Morales and C. M. Lieber, *Science*, 1998, **279**, 208.
- [25] H. Qi, C. Wang and J. Liu, *Adv. Mater.*, 2003, 15, 411.
- [26] S. Vaddiraju, H. Chandrasekaran and M. K. Sunkara, *J. Am. Chem. Soc.*, 2003, 125, 10792.
- [27] Charles Kittel and Herbert Kroemer., *Thermal physics*, W. H. Freeman & Company, London, 2000, p. 78. (ISBN 0-7167-1088-9)
- [28] Irving Langmuir, *Phys. Rev.*, 1913, **2**, 329.
- [29] W. C. Tsai, S. J. Wang, C. L. Chang, C. H. Chen, R. M. Ko, B. W. Liou, *Europhys. Lett.*, 2008, **84**, 16001.
- [30] M. T. Chang, L. J. Chou, Y. L. Chueh, Y. C. Lee, C. H. Hsieh, C. D. Chen, Y. W. Lan, and L. J. Chen, *Small*, 2007, **3**, 658.
- [31] Y. Baek and K Yong, *J. Phys. Chem.*, 2007, **111**, 1213.
- [32] M. Trapatseli, D. Vernardou, P. Tzanetakis and E. Spanakis, *Acs Appl. Mater. Inter.*, 2011, **3**, 2726.
- [33] X. L. Liu, M. Song, S. L. Wang and Y. H. He, *Physica E*, 2013, **53**, 260.
- [34] S. L. Yue, H. Y. Pan, Z. Y. Ning, J. B. Yin, Z. X. Wang and G. M. Zhang, *Nanotechnology*, 2011, **22**, 115703.
- [35] F. H. Chu, C. W. Huang, C. L. Hsin, C. W. Wang, S. Y. Yu, P. H. Yeh and W. W. Wu, *Nanoscale*, 2012, **4**, 1471.
- [36] H. Shi, K. Yu, F. Sun and Z. Q. Zhu, *CrystEngComm*, 2012, **14**, 278. R. V. Kashid, D. J. Late, S., S. Chou, Y. K. Huang, M. De, D. S. Joag, M. A. More and V. P. Dravid, *Small*, 2013, **9**, 2730.
- [37] S. L. Chen, P. Z. Ying, L. Wang, G. D. Wei, J. J. Zheng, F. M. Gao, S. B. Su and W. Y. Yang, *J. Mater. Chem. C*, 2013, **1**, 4779.
- [38] J. Q. Xu, G. H. Hou, T. K. Mori, H. Q. Li, Y. R. Wang, Y. Y. Chang, Y. S. Luo, B. H. Yu, Y. Ma and T. Y. Zhai, *Adv. Funct. Mater.* 2013, **23**, 5038.
- [39] L. A. Valentín, J. Carpena-Nuñez, D. Yang and L. F. Fonseca, *J. Appl. Phys.*, 2013, **113**, 014308.
- [40] B. R. Huang, , J. C. Lin , T. C. Lin and Y. J. Chen, *Appl. Surf. Sci.*, 2014, **311**, 339.
- [41] C. L. Jiang, S. J. Liu, X. C. Chen and S. M. Yu, *CrystEngComm*, 2014, **16**, 8646.
- [42] I. Boscolo, S. Cialdi, A. Fiori, S. Orlanducci, V. Sessa, M. L. Terranova, A. Ciorba and M. Rossi, *J. Vac. Sci. Technol. B*, 2007, **25**, 1253.
- [43] F. Liu, Z. J. Su, W. J. Liang, F. Y. Mo, L. Li, S. Z. Deng, J. Chen and N. S. Xu, *Chin. Phys. B*, 2009, **18**, 2016.

- [44] J. Chen, S. Z. Deng, J. C. She, N. S. Xu, W. X. Zhang, X. G. Wen, and S. H. Yang, *J. Appl. Phys.*, 2003, **93**, 1774.

Table and Figure captions

Table I. Comparison table of the field emission properties of the WO_3 nanowires by different growth methods.

Figure 1. Schematic diagram of the synthesis procedures of the WO_3 nanowire patterns.

Figure 2. (a) Digital photo of the WO_3 nanowire patterns on the glass substrate. (b, c) Low and high magnification SEM images of the sample. (d, e) Top-view and side-view of the nanowires in the pattern. The inset gives the cross-section image of a nanowire.

Figure 3. (a) Typical Raman spectroscopy of the WO_3 nanowires. (b, c) Low- and high-magnification TEM image of a WO_3 nanowire. The inset is the corresponding electron diffraction pattern. And the HRTEM image (Fig. 3(a)) corresponds to the region referred by the black circle in Fig. 3(b).

Figure 4. The SEM images of the samples using different W sources. (a) W plate with a 1 mm thickness. (b) Continuous W film with a thickness of 600 nm. (c) Patterned W film

Figure 5. The morphology of the samples using different width of W film. (a) 500 μm . (b) 250 μm . (c) 70 μm . The inset images are their corresponding high-magnification SEM images.

Figure 6. Schematic illustration of the SVS mechanism. (a) ~ (d) Four growth stages of WO_3 nanowires are respectively evaporation, transportation, nucleation and crystallization.

Figure 7. Field emission properties of the prepared WO_3 nanowire patterns. (a) Schematic diagram of field emission measurement system. (b) Field emission image of the WO_3 nanowire arrays on a 3.5 inch substrate. (c) Field emission current density versus electric field (J-E) curve of the sample. The corresponding FN plots are given in the inset. (d) Emission stability curve of the sample.

Preparation method	Growth temperature (°C)	Pressure	Aspect ratio	Patterned growth	Turn-on field (V/μm)	Ref.
Thermal oxidation	700	66 Pa	10	No	4.7	[29]
Thermal oxidation	750	atmospheric pressure	330	No	1.8	[25]
Thermal evaporation	800	1.3 Pa	200	No	6.4	[30]
Thermal evaporation	900~1100	13.3 Pa	~100	No	4.8	[31]
Hydrothermal deposition	110	high pressure	~10	-	11	[32]
Chemical vapor deposition	950	atmospheric pressure	250	-	7.1	[33]
Thermal evaporation	780	~500 Pa	10	-	~7	[34]
Thermal oxidation	550	2 Pa	40	Yes	25	[5]
SVS method	540	atmospheric pressure	~200	Yes	2.9	This study

Table I

(Z. Xu et al., *submitted to CrystEngComm*)

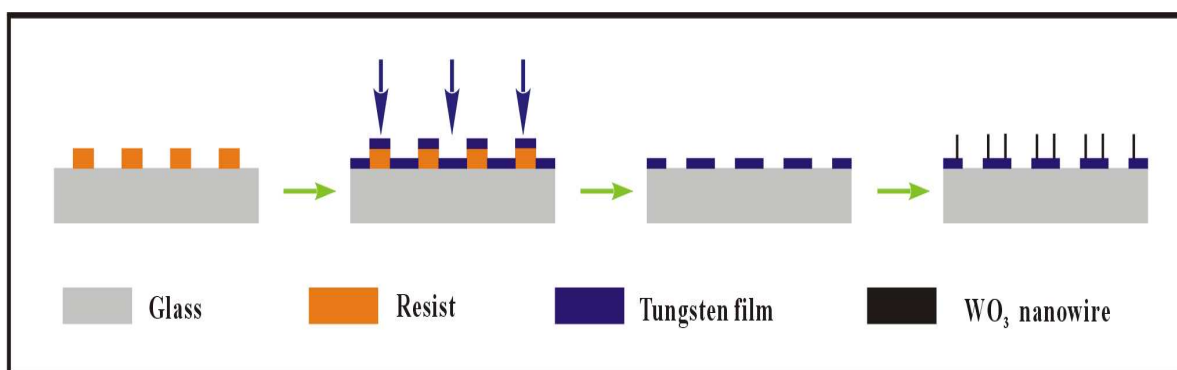


Figure 1

(Z. Xu et al., *submitted to CrystEngComm*)

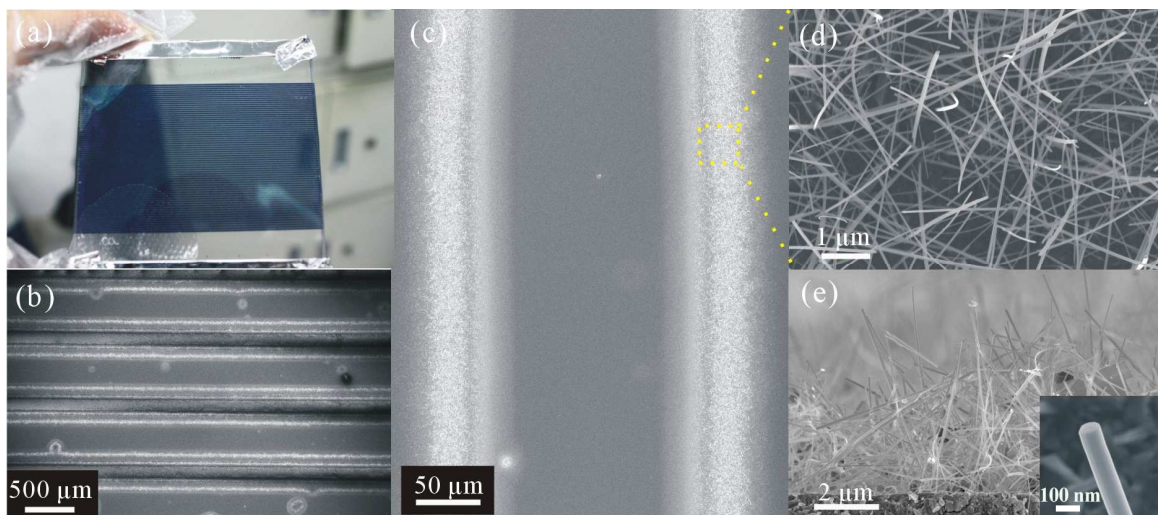


Figure 2

(Z. Xu et al., *submitted to CrystEngComm*)

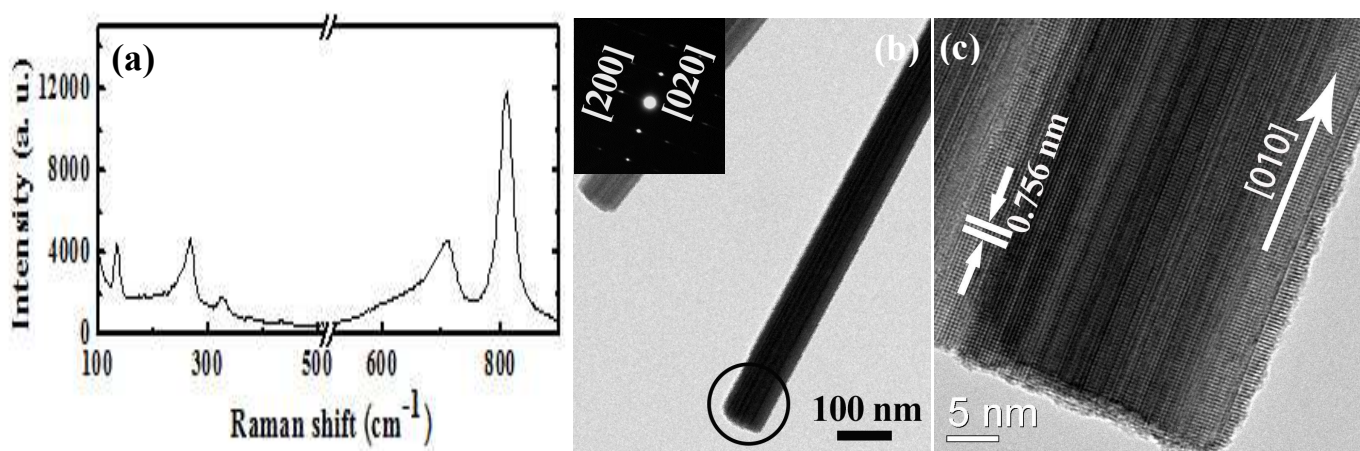


Figure 3

(Z. Xu et al., *submitted to CrystEngComm*)

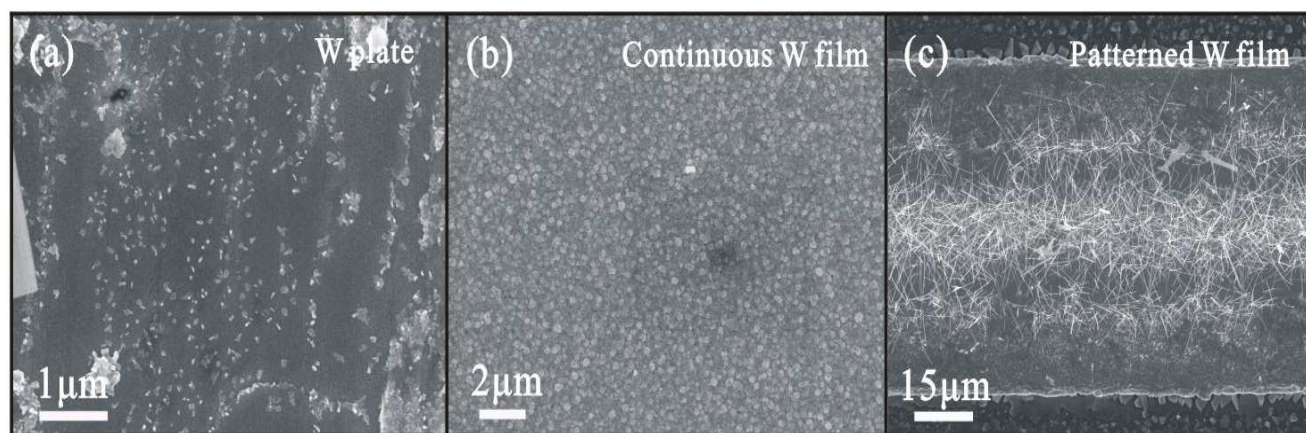


Figure 4

(Z. Xu et al., *submitted to CrystEngComm*)

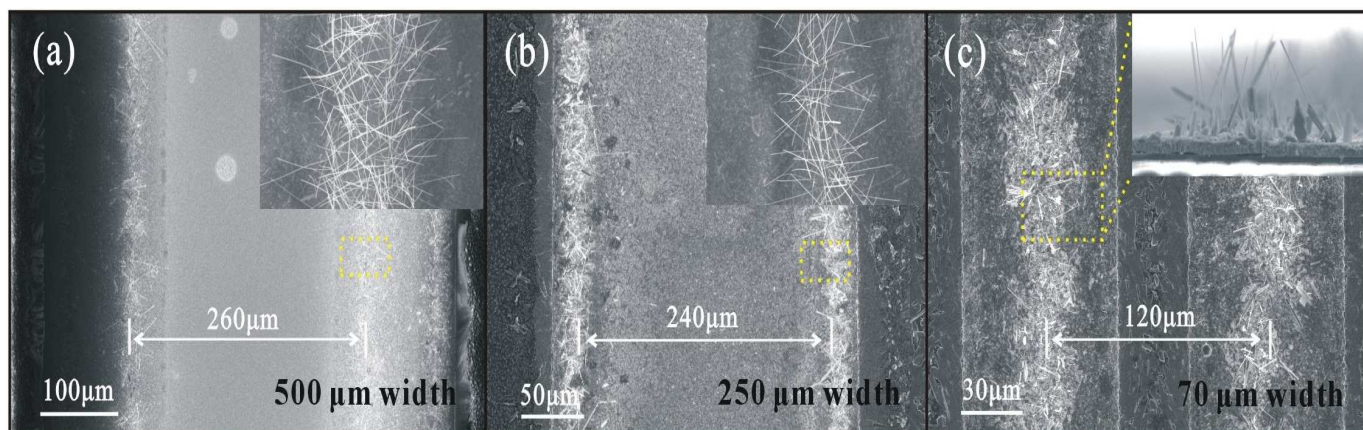


Figure 5

(Z. Xu et al., *submitted to CrystEngComm*)

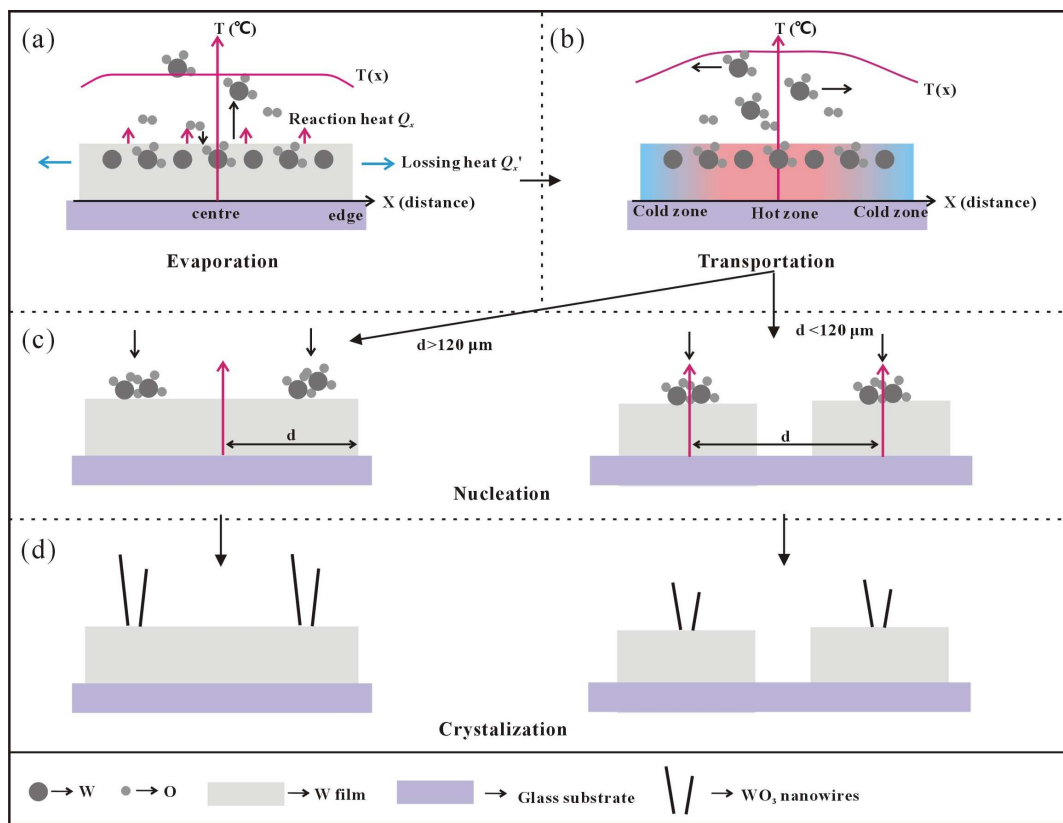


Figure 6

(Z. Xu et al., *submitted to CrystEngComm*)

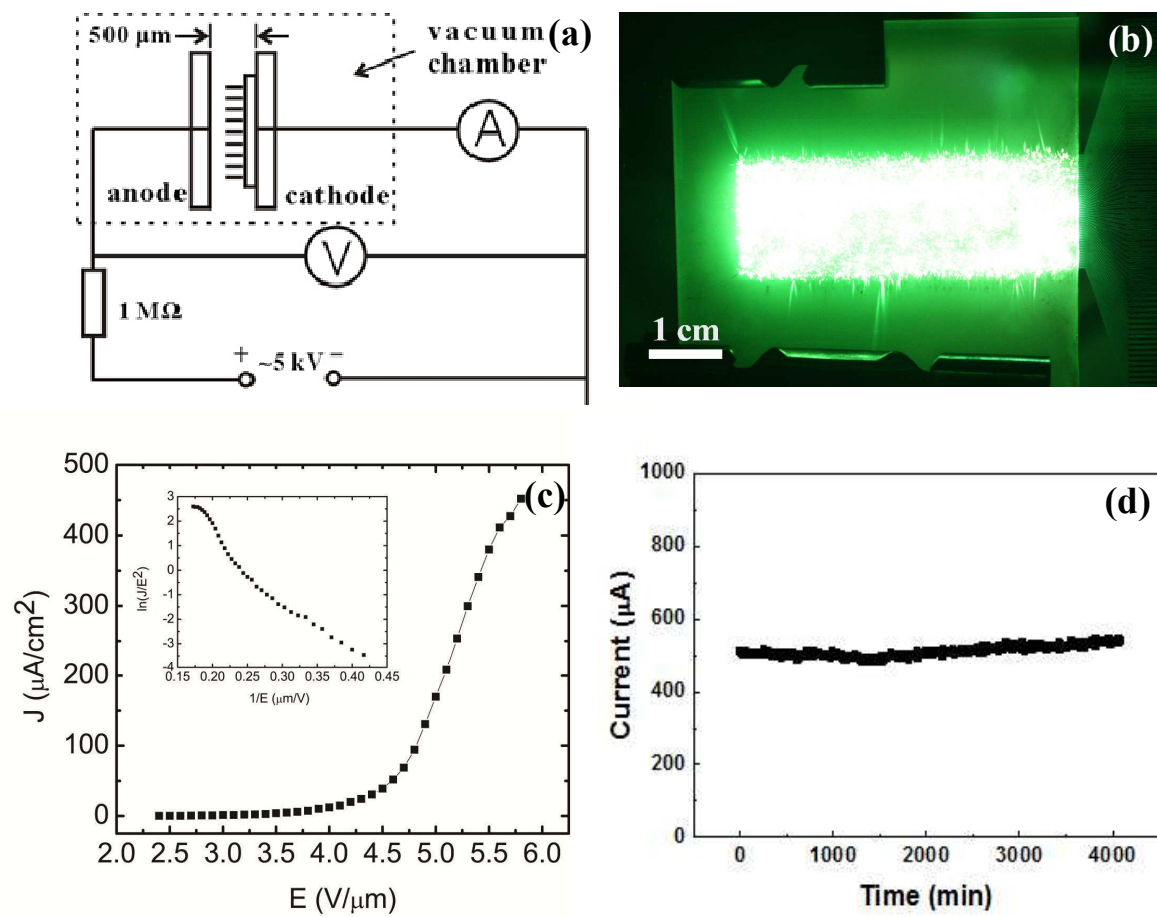
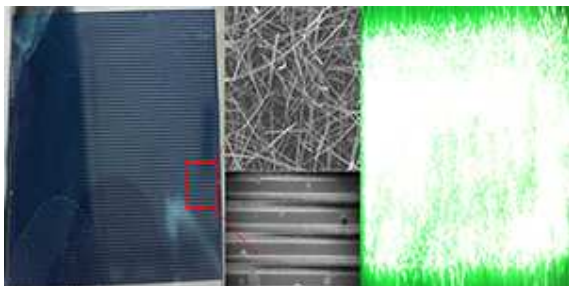


Figure 7

(Z. Xu et al., *submitted to CrystEngComm*)



(Figure for Table of Contents in CrystEngComm)

A novel SVS technique is used to prepare cathode WO_3 nanwire arrays with excellent emission properties on glass substrate.